ELSEVIER

International Journal of Heat and Fluid Flow 20 (1999) 302–310

International Journal of HEAT AND FLUID FLOW

www.elsevier.com/locate/ijhff

Experiments on local heat transfer in a rotating square-ended U-bend

H. Iacovides *, D.C. Jackson, G. Kelemenis, B.E. Launder, Y.M. Yuan

Department of Mechanical Engineering, UMIST, P.O. Box 88, Manchester M60 1QD, UK

Abstract

The paper reports measurements of local heat-transfer coefficients and the associated velocity field measured in turbulent flow through a square-ended U-bend which may be rotated in orthogonal mode. The flow thus has close generic similarities with that arising in the internal cooling passages of modern gas turbine blades. While for no rotation, the separation ahead of the flat end wall of the U-bend provokes an unstable non-repeating flow pattern, the secondary flow created by the duct's rotation gives rise to a strong stable vortex originating near the upstream trailing side of the duct and terminating on the downstream leading side. Within and immediately downstream of the U-bend the corresponding heat transfer data exhibit a significant effect of the rotation of the heat-transfer levels which can be linked with changes in the associated velocity and turbulence field.

Notation

c_p	specific heat capacity
D_h	duct hydraulic diameter
h	coefficient of wall heat flux
k	thermal conductivity
m	mass flow rate
Nu	Nusselt number
P	duct perimeter
Pr	fluid Prandtl number
q	rate of heat transfer
Re	flow Reynold number ($\equiv W_B D_h/v$)
R_i	duct inner radius
Ro	rotation number ($\equiv \Omega D_h/W_B$)
T	temperature
W	axial velocity
z	axial direction
v	fluid kinematic viscosity
ρ	density
τ	thermal time constant of duct wall
Ω	duct rotational speed

Subscripts

B	bulk
w	wall

1. Introduction

The demand to improve the efficiency and power output of gas-turbines has led engine designers to seek continuously to raise operating temperatures. In order to preserve the structural integrity of rotating blades, elaborate cooling systems have evolved in which relatively cool air is bled from the compressor and fed, through the central shaft, to cooling passages inside the turbine blades and nozzle guide vanes. The flow inside these cooling passages is complex and highly three-dimensional, influenced by the presence of sharp U-bends, artificial rib-roughness and by the rotation of the blades. In order to optimize the cooling process, the engine designer needs to have accurate information on the detailed flow development and its effects on local wall heat transfer. Because of the complex shapes of the cooling passages and the presence of rotation, most of the experimental heat-transfer data available until recently, though of considerable value, were nevertheless confined to perimetrally-averaged values. Moreover, due to the lack of detailed data on local flow and heat transfer, it has neither been possible to gain a clear understanding of the hydrodynamic and thermal behaviour in these passages nor to develop and validate numerical flow solvers that can be reliably used for the simulation of blade cooling flows and the consequent thermal stresses that arise.

For the case of non-rotating U-bends, Ekkad and Han (1995) Ekkad and Han (1997) have recently reported detailed measurements of local Nusselt number in smooth and ribbed square-ended ducts using the transient liquid-crystal technique developed by Ireland and Jones (1985). Subsequent studies by Rau et al. (1998) have limited attention to the straight sections of ribbed ducts measuring the Nusselt number by the stationary liquid-crystal method and obtaining details of the corresponding flow field by way of a parallel LDA exploration.

In the case of rotating duct flows, the main reason for the lack of detailed flow measurements has been the fact that, in order to approach the engine-operating conditions using air as the working fluid, experimental models have to rotate at thousands of revolutions per minute, which inevitably limits the size of the experimental models. To overcome this problem, a rotating flow facility has been developed at

* Corresponding author. E-mail: h.iacovides@umist.ac.uk.

0142-727X/99/$ – see front matter
PII: S0142-727X(99)00019-3

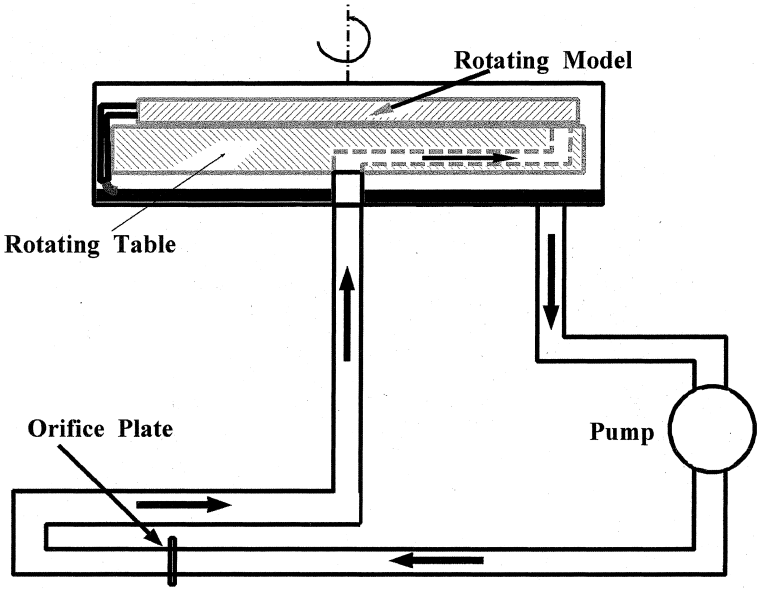

Fig. 1. Rotating flow water rig.

UMIST, Fig. 1, which uses water as the working fluid. As a result, the rotation numbers arising in cooling passages can be reproduced at considerably lower rotational speeds, allowing the use of larger experimental models, with model cooling passages typically 50 mm in diameter. This in turn, enables the collection of point values of flow and thermal data.

Our initial investigations focused on flow through round-ended U-bends, rotating orthogonally about an axis parallel to that of the bend curvature. This resulted in LDA measurements, first for a U-bend with smooth walls (Cheah et al., 1996) and then for U-bends with staggered ribs along the upstream and downstream sections (Iacovides et al., 1998a, b). In smooth U-bends the flow along the inner wall was found to separate around 90° into the bend. The separation bubble extended nearly two diameters into the downstream section, raising substantially turbulence levels after the second half of the bend. Because of the curvature-induced secondary motion the flow was also found to be highly three-dimensional. Orthogonal rotation at a rotation number Ro of ±0.2 was found to have a marked effect on the flow development, increasing the length of the separation bubble, when the Coriolis and curvature forces acted in the same direction and speeding up the downstream recovery when the Coriolis and curvature forces opposed one another.

The present paper continues our investigation of flow through U-bends relevant to blade cooling, but shifts its emphasis to the measurement of wall heat-transfer coefficients. The rotating-flow rig has been extensively modified to enable uniform heating to be supplied and data of local wall temperature in this rotating system to be extracted. For the present we can report data only for the smooth square-ended U-bend; the case of ribbed U-bends will be reported in a future publication.

2. Apparatus and procedure

2.1. Apparatus

As shown in Fig. 1, the rotating rig consists of a motor-driven turntable mounted in a 1.22 m diameter water tank. Experimental models of blade-cooling passages are mounted on the turntable so that the axis of rotation is normal to the main flow direction, resulting in an orthogonal-mode rotation. Water is circulated in a closed loop system, where it is first pumped through a long orifice plate section. It then arrives, through a vertical pipe, below the centre of the rotating turntable and enters an internal passage built into the rotating turntable, through which it enters the experimental model mounted on the turntable. The outflow is discharged into the open water tank. A combination of fine wire meshes and a honeycomb section is located at the entrance to the experimental model, to ensure uniform and symmetric entry conditions. The turntable can be driven at any required speed, up to 250 rpm in either direction. A feedback control circuit utilises the input from a rotary encoder on the drive shaft to control precisely the rotational speed. Further details of this rig have been given in Cheah et al. (1996) and Iacovides et al. (1998a).

2.2. Measurements

As reported in our earlier publications, to record velocity data on the rotating flow rig, a stationary fibre-optic probe was positioned above the experimental model and collected LDA measurements of the instantaneous velocity as the model rotated past it. Here the emphasis is placed on the description of how the liquid-crystal technique was used to measure the coefficient of heat transfer.

As documented by Hippensteele et al. (1993) and Ireland and Jones (1985), Jones et al. (1992) and later workers, the molecular structure of thermochromic liquid crystals, over a certain temperature range, depends on temperature. Changes in molecular structure in turn affect the wavelength of visible light absorbed by the liquid crystals and hence, over this temperature interval, the colour of the liquid crystals can be used to determine their temperature. In heat-transfer experiments where air is the working fluid, most groups have adopted the transient liquid-crystal technique, in which the surface under investigation is covered with a layer of liquid crystals and is exposed to a hot air stream. As the surface temperature gradually rises from the initial ambient conditions, the movement of the colour contours of the liquid crystals along the surface is monitored. Then, from the time needed for the wall temperature at any point to rise from its initial value to that of the crystal-colour-change temperature,

the solution of the one-dimensional transient heat-conduction equation enables the value of the heat-transfer coefficient h, to be determined.

In the case of water, the higher coefficients of heat transfer involved lead to a substantially shorter thermal time constant ($\tau \equiv \rho_w c_{pw} k_w / h^2$). Surface temperatures thus rise too rapidly to measure accurately. The *steady-state* liquid-crystal technique has therefore been adopted for our investigations. The surfaces of the experimental model are covered with a thin, electrically heated, stainless steel foil, which provides a constant-heat-flux thermal boundary condition. A thin layer of liquid crystals is then applied over the surface of the heating foil. Once steady thermal conditions are reached, the resulting colour contours are also contours of known wall temperature, determined through a prior calibration, under conditions of uniform wall heat flux. Electrical measurements provide the wall heat flux, q_w and, from the overall energy balance, the fluid bulk temperature, T_B, can also be determined:

$$mc_p(dT_B/dz) = Pq_w, \tag{1}$$

where z is the streamwise coordinate and P the heated perimeter.

The local Nusselt number along each colour contour can then be calculated, since

$$N \equiv (q_w D_h)/[k(T_w - T_B)]. \tag{2}$$

By repeating the above procedure for a number of heating rates, a detailed mapping of the local Nusselt number over each heated wall can be constructed.

First, a number of cases involving heat transfer in stationary passages, with air as the working fluid, were investigated. These enabled the software necessary for the digital processing of the images of the heated surfaces to be developed. In all cases, micro-encapsulated liquid crystals manufactured by Merck were employed, with a nominal colour-change band between 29.5°C and 31°C, for the entire visible spectrum, and a nominal change of 0.1°C across the yellow colour, which was used to determine the wall temperature. At each heating rate, the image of the resulting colour contours was recorded using a CCD camera, digitized and stored on a PC. The digitized image was then converted into a hue-saturation-and-intensity format and the pixels with a hue value corresponding to that of the yellow colour were identified. Software developed for this study then corrected the co-ordinates of the selected pixels, accounting for distortions caused by the camera lens and the angle between the camera line of sight and the orthogonal to the measurement surface. The information from each image was thus reduced to provide the co-ordinates of the constant-wall-temperature contour. The value of h along the contour line was then calculated, using Eqs. (1) and (2). Finally, the contour lines produced by different heating rates were brought together and, through interpolation, the continuous variation of the Nusselt number over the heated surface was produced.

With water as the working fluid, because of its different fluid properties, the time required for thermally steady conditions to be reached is greatly reduced, but considerably higher power levels were needed to achieve accurate measurements of temperature difference. Moreover, the nominally waterproof liquid crystals were found to absorb water, which made the resulting images unclear. The 15 μm thick stainless-steel foil selected for these investigations was able to produce power density levels up to 80 kW/m^2, which preliminary calculations showed to be necessary. In order to prevent exposure of the liquid crystals to the water, the arrangement shown in Fig. 2 was employed, in which the liquid crystals were enveloped between the stainless steel foil and the perspex wall of the passage. The colour contours were viewed through the perspex wall, by a camera located opposite to the heated wall. As can also be seen in Fig. 3, illumination, necessary for the colour contours to become visible, was provided by two power efficient halogen lamps on either side of the camera. This arrangement was first tested for water flow through a heated stationary passage.

For the rotating passages the additional problems of supplying the electrical power and recording the resulting images in a rotating frame of reference had to be addressed. As is indicated in Fig. 4, six power slip rings were used to transmit the electrical power to different sections of the heated model, each one capable of transmitting up to 2.5 kW. Just the pressure and suction faces of the duct were heated. As noted in Fig. 9, there is a small unheated strip half way around the bend. The camera was also mounted on the rotating turntable and its signal was fed to a PC through separate slip rings. The illumination lamps were likewise powered through slip rings, from a heavy duty battery. The possible effect of a centrifugal field on the liquid-crystal response has been raised by several authors. However, a recent joint-study by two research groups, Camci et al. (1998) concluded that "even for centripetal accelerations in excess of 10^4 g there is no significant effect of rotational speed". In our tests, conducted at rotation speeds of about 45 rpm, acceleration levels were only 10 g.

Measurements are reported here for the square ended smooth U-bend of square cross section shown in Fig. 2. LDA

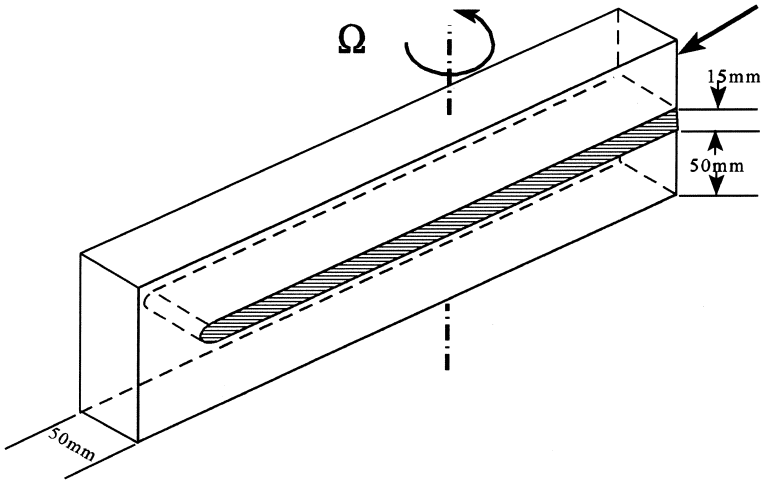

Fig. 2. The configuration examined.

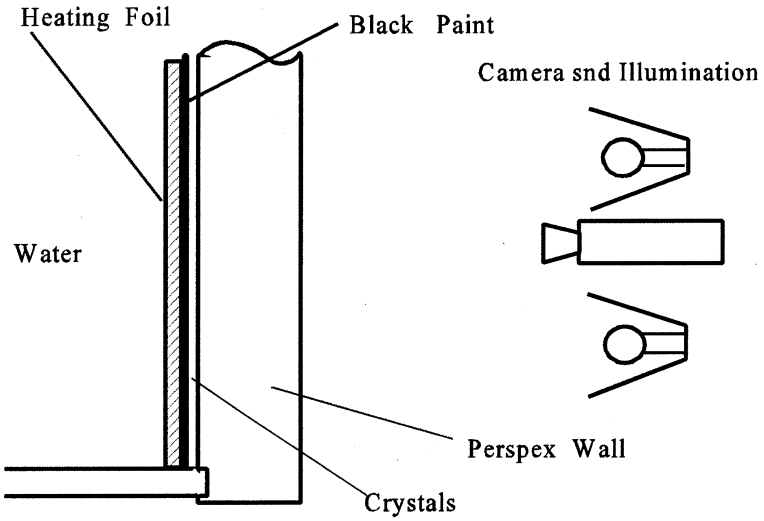

Fig. 3. Arrangement of liquid crystals in water-cooled passages.

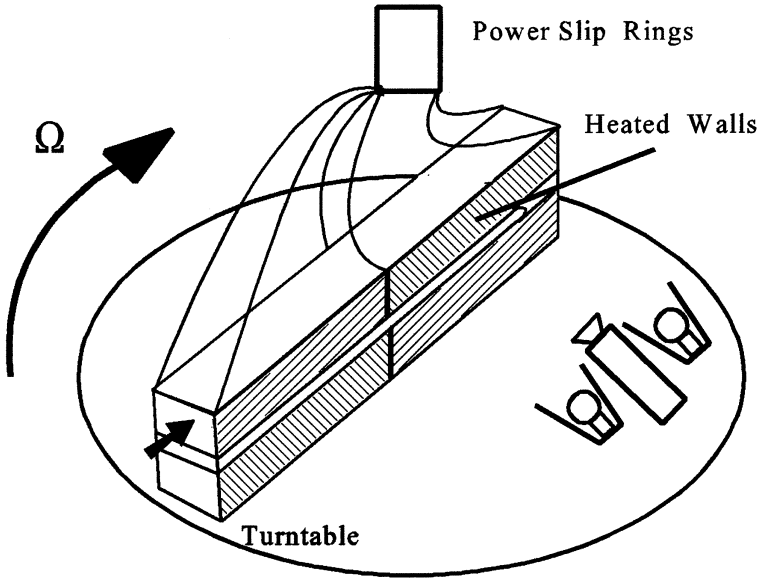

Fig. 4. Heating and monitoring arrangements for rotating passages.

and heat-transfer measurements are presented for both rotating and stationary conditions. The ratio between the bend inner radius and the duct diameter, R_i/D, is 0.15. For the flow measurements the flow Reynolds number is 100 000 and for the heat-transfer measurements 30 000. While ideally both the flow and the thermal measurements would have been obtained at the same Reynolds number, because of the high heat transfer rates required to maintain a reasonable temperature difference (10°K), the flow Reynolds number in the heat-transfer experiments had to be reduced. In both cases the rotation number ($R_o \equiv \Omega D_h/W_B$) is 0.2 and the working fluid is water, Pr = 5.9. As indicated, only the two flat vertical walls of the duct were heated.

3. Presentation and discussion of results

Fig. 5, shows the mean flow development along the geometrical symmetry plane of the smooth, square-ended U-bend for no rotation. The curvature-induced separation bubble along the inner wall is considerably smaller than that observed in the smooth round-ended U-bend (Cheah et al., 1996), because in the present geometry, the effective cross-sectional area reduces over the second half of the bend, imposing an overall acceleration on the flow. However, additional separation bubbles are formed in the corners.

Vector plots on a plane normal to the geometric symmetry plane, mid-way between the inner and outer walls, shown in Fig. 6, indicate that, within the bend, the flow becomes non-symmetric. Sometimes a mirror image of the flow pattern shown was established. Flow visualisation tests, using dye injection, suggested that the corner separation bubbles make the flow within the square-ended U-bend unstable, which destroys the flow symmetry. Downstream of the bend, however, the flow recovers to a symmetric form. The curvature-induced secondary motion transports the faster fluid to the near-wall (vertical wall) regions, leaving the slower fluid in the duct centre. Measurements of the fluctuating field, not shown here,

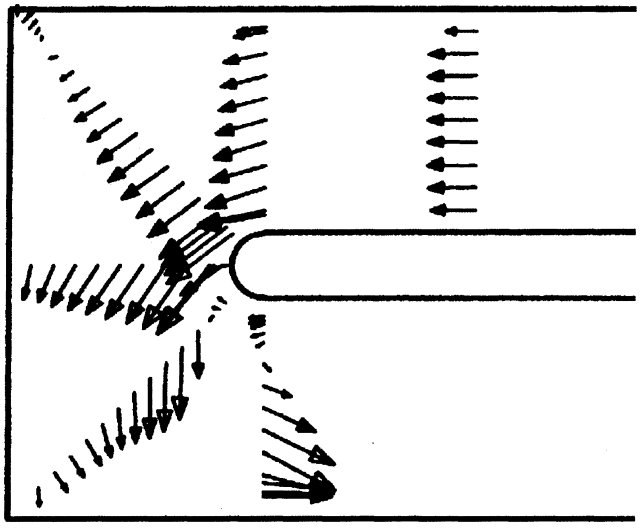

Fig. 5. Mean flow development along the geometrical symmetry plane for Ro = 0.

reveal that in the exit region of the square-ended U-bend, turbulence levels are higher than those found in the round-ended case (Cheah et al., 1996).

When the passage rotates orthogonally about an axis normal to that of curvature, the geometrical symmetry plane is no longer (even ideally) a plane of flow symmetry. Vector plots obtained at the 90° location of the bend, shown in Fig. 7, indicate that a strong vortex is formed along the leading side of the rotating passage, which, so far as the upstream flow is concerned, is the suction side. Dye injection tests have also confirmed the presence of this vortex, which starts near the leading side (which for the upstream flow is the suction side) of the rotating passage, but over the second half of the bend crosses to the trailing side which, over the downstream region, becomes the suction side of the duct.

The flow development in the downstream region, is mapped in detail in the vector plots of Fig. 8. At the exit plane along the inner wall (C), the flow separates along the trailing (now the suction) side, while along the leading side the flow is strongly accelerated. At the middle of the exit plane (B), there is no flow separation along the trailing side, though there is still a considerable increase in velocity across the duct, from the trailing to the leading side. Near the upper wall (A), the velocity is high and nearly uniform right across the duct. The cross-duct motion at the exit plane indicates that a single streamwise vortex is present which, along the inner wall and the duct centre, convects the fluid from the leading to the trailing side, and along the outer wall returns the fluid to the leading side. This is consistent with the single vortex found at the 90° plane. Because of this secondary motion, the flow along the leading side re-attaches less than one diameter downstream of the bend exit and further downstream the faster fluid is transported from the leading to the trailing side which, in the downstream section is the suction side. Even seven diameters downstream from the bend exit, the faster fluid is still along the suction side, which is the opposite from what is found in fully developed flow in a rotating straight duct. It may thus be concluded that when the Coriolis and curvature forces are normal to each other, the resulting flow is not only more complex than when the two forces are co-aligned, but that the effects of the bend on the flow persist further downstream.

The corresponding Nusselt number contours for stationary and rotating conditions, at a Reynolds number of 30 000, are displayed in Fig. 9. Under stationary conditions, they show that upstream of the bend the Nusselt number is uniform. Its level is about 25% higher than that returned by the experimental correlation recommended by Kays and Crawford (1980) for fully-developed flow for fluids with Prandtl numbers between 1 and 20, Eq. (3), for fully-developed flow at this Reynolds and Prandtl number:

$$N = 0.0155Re^{0.83}Pr^{0.5}. \quad (3)$$

The turbulence intensities measured in the upstream section are, however, also higher than those encountered in fully-de-

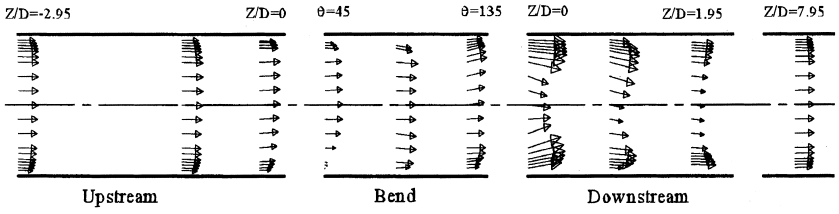

Fig. 6. Mean flow development along circumferential mid-plane for Ro = 0.

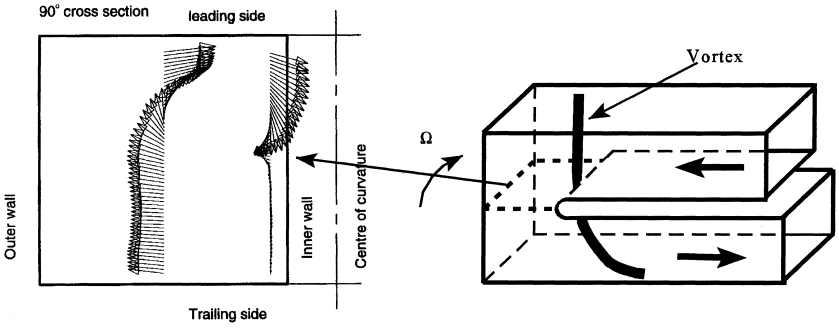

Fig. 7. Secondary motion at the 90° plane of a rotating square-ended U-bend, Ro = 0.2.

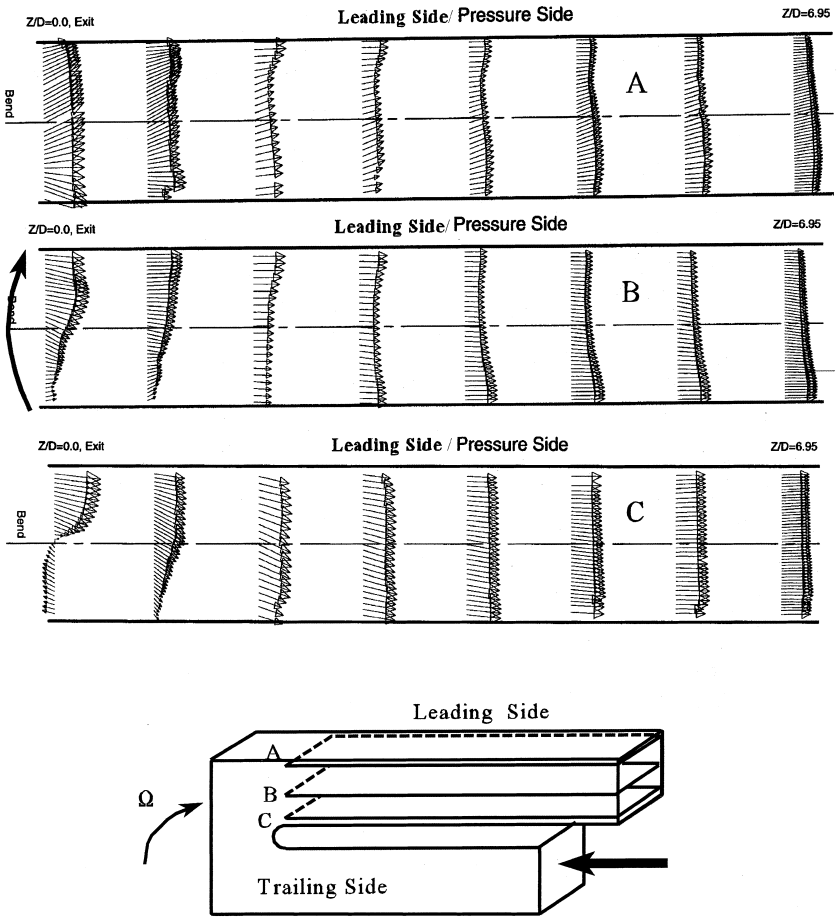

Fig. 8. Mean flow development along indicated circumferential planes, downstream of rotating square-ended U-bend, Ro = 0.2.

veloped flow in a straight duct, which may explain this discrepancy.

Nusselt numbers rise within the U-bend, over the first half of the bend the highest levels being along the end-wall corner. Higher turbulence levels due to flow separation in the corner is the most probable cause. The levels of Nusselt number rise even further over the second half of the U-bend, especially at the bend exit where peak levels are twice as high as those upstream. These high values persist over the first downstream diameter, where the LDA measurements have shown that the secondary motion transports the high momentum fluid to the heated walls; they then gradually reduce. Even after four diameters, however, levels of Nu are still higher than the upstream values.

Under rotating conditions, along the leading side, (Ro = −0.2), heat transfer levels in the upstream section (which for the leading side is the suction side) are found to increase in the corner regions. This is consistent with the expected, Coriolis-driven, secondary motion, which, along the unheated walls, would transport cooler fluid to the corner regions of the leading side, as shown in Fig. 8. At the bend entry, there is an abrupt rise in heat-transfer coefficient, which is markedly stronger than that observed in the stationary case. Two regions of local maxima are formed over the first half of the U-bend, one near the inner wall and one along the end-wall corner. These higher levels of Nu in the bend entry region of the leading side, are consistent with the strong vortex that was found by the LDA and flow-visualisation experiments in this region, shown in Fig. 7.

Over the second half of the bend, where the vortex is observed to turn away from the leading side, the high levels of heat transfer near the inner wall disappear and the higher heat transfer regions are now along the end-wall and outer-wall corners. The region of low Nusselt number near the inner-wall corner at and downstream of the bend exit coincides with the region over which, according to the LDA measurements in Fig. 8, the cross-duct motion is directed away from the leading side. Similarly, the higher levels of Nusselt number measured along the outer wall corners over the same region, appear to be caused by the fact that, near the outer wall, the cross-duct motion is directed towards the leading side. Further downstream of the bend exit, beyond the first two diameters, in contrast to the stationary case, Nusselt number levels in the middle of the leading side are lower than those in the corner regions. As can be seen in Fig. 7, along the leading side, after the first two downstream diameters, the flow along the inner wall is faster than that along the mid-plane. While the flow near the outer wall, over the same region, does not appear to be faster than that along the mid-plane, LDA data, not presented here, show that near the outer wall, the turbulence intensities along the cross-duct direction are higher than those near the mid-plane.

Along the trailing side, heat-transfer levels in the upstream section (for which the trailing side is the pressure side) are uniform and, over the first half of the bend, the increase in Nusselt number is not as strong as that observed on the leading side (even in the absence of rotation). This is also consistent with the LDA measurements and flow visualization observations

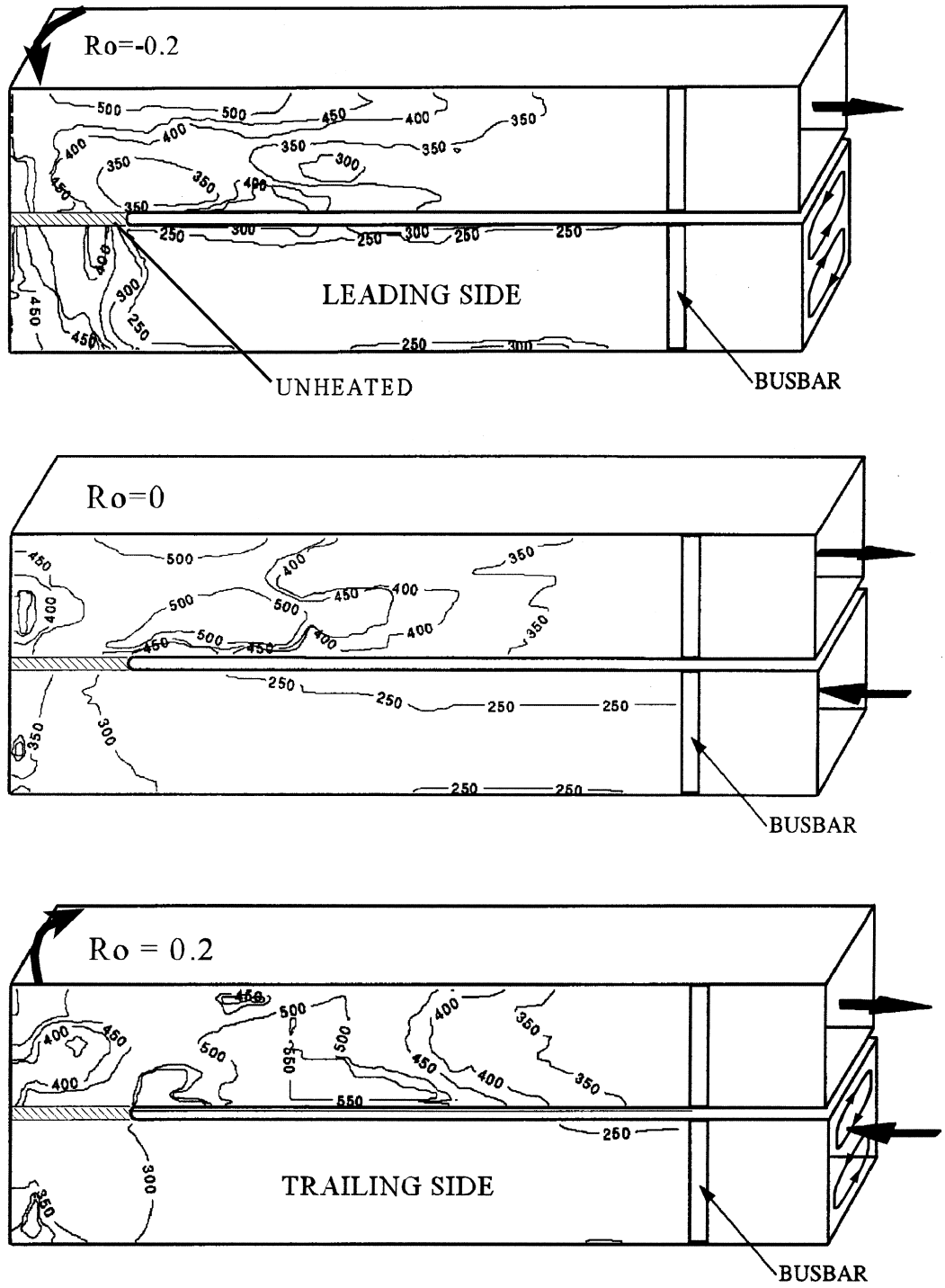

Fig. 9. Nusselt number contours. Re = 30 000 and Pr = 5.9.

within the U-bend, shown in Fig. 7. Over the second half of the bend, there is a marked rise in Nusselt number as the vortex turns from the leading to the trailing side. At, and immediately downstream of, the bend exit the effects of the separation bubble along the inner wall, shown in the measured vector plots in Fig. 8, are clearly evident. When the flow re-attaches, at about one diameter from the bend exit, a further increase in local Nusselt number takes place, resulting in values higher than those measured either along the leading side or, indeed, along the sides of the stationary U-bend.

The variation of local Nusselt number along the trailing side appears to be similar to that on the stationary side, though the actual levels are different. This is probably because the flow development along the trailing side of the rotating square-ended U-bend is similar to that for the stationary case. One notable difference is, of course, the larger curvature-induced separation bubble at the bend exit, for the trailing side which causes the higher Nusselt number levels in the downstream region. The distribution of the local Nusselt number along the leading side of the rotating U-bend is, on the other hand,

different from that of the stationary case for two reasons in particular: the formation of the strong vortex at the bend entry and the fact that, at the bend exit, instead of flow separation, there is strong flow acceleration along the inner wall.

The variation of the side-averaged value of the Nusselt number along the square-ended U-bend, under both stationary and rotating conditions, presented in Fig. 10, enables us to quantify more easily the effects of curvature and rotation on wall heat transfer. For the stationary case, the U-bend raises the Nusselt number levels by a factor of two, compared to the upstream values. This maximum level is reached at about 0.6 diameters after the bend exit. Even after four diameters downstream of the bend exit, Nusselt numbers are about 20% higher than those upstream. Rotation effects on the mean Nusselt number upstream of the bend appear to be small, though, as expected, heat-transfer coefficients are augmented along the pressure side ($Ro = 0.2$) and attenuated along the suction side ($Ro = -0.2$). The reason for this apparently weak influence of rotation on wall heat transfer is believed to be the relatively short length of flow development upstream of the bend, about 10 D in total, and the uniform velocity distribution produced by the honeycomb section and wire meshes. Consequently, the boundary layers do not have a sufficient length of flow development. As a result, the Coriolis-induced secondary motion, which arises from the non-uniformity of velocity across the duct, does not become as strong as in fully-developed flow in a rotating duct. Within the first half of the U-bend, as noted in the local Nu contours of Fig. 9, heat-transfer coefficients along the leading side show a rapid rise, 35% higher than for the stationary case, while along the trailing side the Nu levels follow those of the stationary case. Over the second half of the U-bend and over the first diameter downstream, Nusselt-number levels along the trailing side become lower than those of the stationary case by about 20% because of the absence of flow separation. Along the trailing side over the second half of the duct and the first four diameters downstream (as noted earlier) the thermal development is similar to that of the stationary case. However, because of the larger separation bubble at the inner wall, the peak heat-transfer coefficient occurs further downstream (more than one diameter from the bend exit) and is about 10% higher than that of the stationary case.

These comparisons for the square-ended U-bends with smooth walls, have shown how the local flow features caused by strong curvature and orthogonal rotation directly influence the local Nusselt number. The primary influence appears to be that of curvature, increasing the coefficient of local wall heat flux by as much as a factor of two. Even with a short length of upstream flow development, which does not allow the Coriolis-driven secondary motion to reach its full strength, the effects of orthogonal rotation on the local wall heat transfer within and downstream of the square-ended U-bend cannot be ignored. Differences between the levels of Nusselt number along the leading and trailing sides are as high as +45% within the U-bend and −25% downstream.

4. Concluding remarks

The data reported above provide the first *local* measurements of wall heat transfer coefficients in a rotating U-bend. The fact that detailed mean flow and turbulence data are also available means that the data set provides a more complete basis for testing CFD codes and for diagnosing the sources of inadequacies in any turbulence model that may be employed in the codes. It has been shown that specific features in the heat-transfer pattern, including the changes associated with rotation, arise from particular features of the flow field reinforcing the importance of making flow-field as well as thermal measurements.

It is understood that until today the designers of internal cooling passages tend to employ just circumferentially average data as the basis for optimizing their design. The rapid spatial variation of local heat transfer coefficient recorded in this study, however, strongly suggests that, in evaluating thermal stresses in blades and their consequences, account should be taken of these quite severe perimetral variations. Perhaps in addition, with the added knowledge of local values of Nu, redesigning of the blades should be made to minimize these local variations which can only raise the stress concentration levels in an actual turbine blade.

Of course, many current cooling passage designs employ ribs to raise the level of heat transfer measurements. The

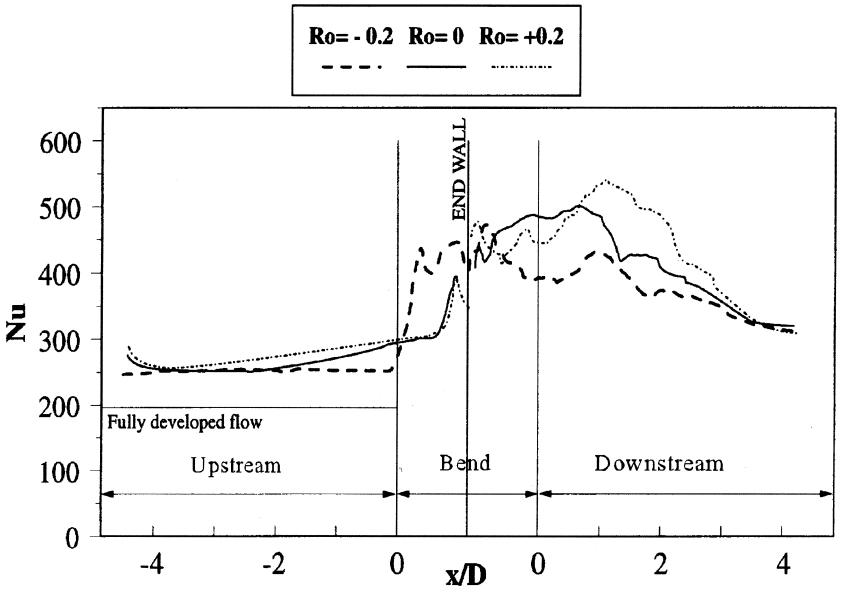

Fig. 10. Side-averaged Nusselt number. $Re = 30\,000$ and $Pr = 5.9$.

authors' own work on this subject will be reported in a future communication.

Acknowledgements

Funding for the work presented has been provided by the EPSRC, ABB (Switzerland), EDF (France), EGT, and Rolls-Royce plc. The authors gratefully acknowledge both the financial support and the expert advice received from this sponsorship. The authors also acknowledge technical support provided by Mr D. Cooper, Mr J Hosker and Mr M. Jackson.

References

Camci, C., Glezer, B., Owen, J.M., Pilbrow, R.G., Syson, B.J., 1998. Application of thermochromic liquid crystal to rotating surfaces. ASME J. Turbomachinery 120, 100–103.

Cheah, S.C., Iacovides, H., Jackson, D.C., Ji, H.H., Launder, B.E., 1996. LDA investigation of the flow development through rotating U-ducts. ASME J. Turbomachinery 118, 590–596.

Ekkad, S.V., Han, J.C., 1995. Local heat transfer distributions near a sharp 180° turn of a 2-pass, smooth square channel using a transient liquid-crystal image technique. J. Flow Visual. Image Process. 2, 285–297.

Ekkad, S.V., Han, J.C., 1997. Detailed heat transfer distributions in 2-pass square channels with rib turbulators. Int. J. Heat Mass Transfer 40, 2525–2537.

Hippensteele, S.A., Russell, L.M., Stepka, F.S., 1993. Evaluation of a method for heat transfer measurements and thermal visualization using a composite of a heater element and liquid crystals. ASME J. Heat Transfer 105, 184–189.

Iacovides, H., Jackson, D.C., Ji, H.H., Kelemenis, G., Launder, B.E., Nikas, K., 1998a. LDA study of the flow development through an orthogonally rotating U-bend of strong curvature and rib-roughened walls. ASME J. Turbomachinery 120, 366–391.

Iacovides, H., Jackson, D.C., Launder, B.E., Yuan, Y.M., 1998b. An experimental study of a rib roughened rotating U-bend flow, in preparation.

Ireland, P., Jones, T.V., 1985. The measurement of local heat-transfer coefficients in blade-cooling geometries. In: AGARD Conference on Heat Transfer and Cooling in Gas Turbines, CP 390, Paper 28.

Jones, T.V., Wang, Z., Ireland, P.T., 1992. Liquid Crystal Techniques, ICHMT. In: International Symposium on Heat Transfer in Turbomachinery, Athens, Greece.

Kays, W.M., Crawford, M.E., 1980. Convective Heat and Mass Transfer, 2nd ed. McGraw-Hill, New York.

Rau, G., Cakan, M., Moeller, D., Arts, T., 1998. The effect of periodic ribs on the local aerodynamic and heat-transfer performance of a straight cooling channel. ASME J. Turbomachinery 120, 368–375.